

Magnetization and spin distribution of single sub-monolayers of MnTe in semiconductor quantum wells

G. Prechtel, W. Heiss, A. Bonanni, and W. Jantsch

Institut für Halbleiter und Festkörperphysik, Universität Linz, Altenbergerstraße 69, 4040 Linz, Austria

S. Mackowski and E. Janik

Institute of Physics, Polish Academy of Sciences, 02-668 Warsaw, Poland

(Received 14 July 2003; published 14 October 2003)

The magnetization of single, ultrathin MnTe layers embedded in nonmagnetic quantum wells is studied by magneto-optical spectroscopy as well as by numerical simulations. It is shown to be proportional to the Zeeman splitting and thus it can be directly deduced from the magneto-optical experiments. The inverse of the experimentally determined magnetization measured as a function of temperature clearly demonstrates deviations from Curie-Weiss behavior due to the antiferromagnetic coupling between the Mn ions. By fitting this temperature dependence, an approximate Mn diffusion profile is obtained for each sample. The fitting procedure takes into account the antiferromagnetic coupling between the Mn ions as well as the exchange interactions between the Mn ions and the photoexcited electrons. For this purpose we have numerically solved the two-dimensional Ising model by a Monte Carlo method giving the magnetization of two-dimensional layers as a function of magnetic field, temperature, and Mn concentration.

DOI: 10.1103/PhysRevB.68.165313

PACS number(s): 78.67.De, 78.55.Et, 75.70.Ak, 75.30.Kz

I. INTRODUCTION

Continuous order-disorder phase transitions are categorized into universality classes depending on a small number of parameters like the symmetry of the ordered phase or the *dimensionality* of the system.¹ Therefore the corresponding order parameter, e.g., the magnetization M in magnetic systems, is expected to behave fundamentally different in systems with different dimensionality. While in semiconductors, three-dimensional magnetic systems are widely investigated,² much less is known about two-dimensional (2D) magnetic arrangements due to several complications. 2D magnetic system can be realized, e.g., by deposition of a well ordered monolayer (ML) or a submonolayer of magnetic atoms atop a nonmagnetic substrate.³⁻⁶ Such an arrangement is, however, not an ideal 2D system, because surfaces are not completely flat and they are contaminated by defects. When the magnetic layer is buried under a cap layer the situation is even worse due to migration during growth, leading to a smeared distribution of the magnetic ions over distances of several ML's.^{7,8} In spite of these disadvantages, in semiconductor heterostructures buried magnetic monolayers are of high interest because (i), they can interact with the spin of free carriers⁹ and thus they can be used for spin manipulation and because (ii), the insertion of magnetic ML's leads to different magnetic properties than observed in epilayers uniformly doped by magnetic ions.^{9,10} Although 2D ordered magnetic systems can be observed also in superlattices,¹¹ in this work we use single magnetic layers in order to explicitly avoid interlayer coupling effects due to long-range magnetic dipole interactions.¹²⁻¹⁴

In particular, we investigate single sub-monolayers of zinc-blende (ZB) MnTe embedded in II-VI semiconductor quantum wells. ZB MnTe forms a fcc Heisenberg system with strongly dominating antiferromagnetic nearest-neighbor exchange interaction. The ground state of bulk MnTe is that

of a type-III antiferromagnet¹⁵ exhibiting a first-order magnetic phase transition at the Néel temperature of $T_N = 66.7$ K.¹⁶ The Mn ions present in the quantum well experience also spin-spin exchange interactions with photoexcited carriers in the s -like conduction band and p -like valence band. This sp - d interaction leads to a strong increase of the exciton spin (Zeeman) splitting, which is directly proportional to the magnetization.^{17,18} Therefore in our magnetic semiconductor heterostructures the magnetization can be probed by magneto-optical spectroscopy.

For a quantitative analysis, the experimental data are compared with numerical results taking into account spin-spin interactions between neighboring magnetic ions as well as sp - d exchange interactions. The latter are included by a fitting procedure whereas the first ones are exactly calculated using a 2D spin- $\frac{1}{2}$ Ising model solved within a Monte Carlo simulation. In particular, the temperature dependence of the magnetization is inspected in samples nominally containing either a complete ML of MnTe or $\frac{1}{2}$ ML MnTe. Fitting the experimental temperature dependencies of the magnetization allows us to determine the actual Mn distribution present in the samples.

II. MAGNETIZATION OF A TWO-DIMENSIONAL, CUBIC MnTe LATTICE

In this section we discuss the simulation of a purely two-dimensional arrangement of magnetic ions with antiferromagnetic exchange interactions as a function of magnetic field, temperature, and concentration of magnetic ions. An appropriate tool to calculate the ground-state energy and magnetization of ZB-MnTe in three dimensions would be to solve the Heisenberg model for spins arranged on a cubic lattice, by taking into account nearest-neighbor and next-nearest-neighbor exchange interactions. The Hamiltonian for this problem is given by¹⁹

$$H = \sum_{ij} J_{ij} \varepsilon_i \varepsilon_j \mathbf{S}_i \mathbf{S}_j - g_s \mu_B \mathbf{B} \sum_i \varepsilon_i \mathbf{S}_i, \quad (1)$$

where J_{ij} is the exchange integral between the magnetic ions at the sites i and j with the spin S_i and $S_j = \frac{5}{2}$, $g_s = 2$ is the Lande factor of the magnetic ions, μ_B is the Bohr magneton, B represents the external magnetic field, and $\varepsilon_i = 0$ or 1 allows us to change the population of site i . As an approximation, we take into account only the nearest-neighbor exchange interaction, and set $J_{ij} = J$. Furthermore, we are interested in MnTe monolayers embedded in CdTe quantum wells with CdMgTe barriers. This allows us to make two further simplifications: On one hand, we treat a purely two-dimensional lattice with magnetic Mn ions. On the other hand, we allow for the calculation of the magnetic ordering at arbitrary magnetic field and temperature only two directions of the Mn spins, which means that we use the Ising model instead of the Heisenberg model. The Ising model is an appropriate description for our case, because the MnTe lattice embedded in the CdTe quantum well is considerably distorted due to the lattice mismatch of 2.3% between CdTe and MnTe. The larger lattice constant of CdTe causes an elongation of the MnTe unit cell in lateral directions (x and y) and a shortening in the z direction. The exchange interaction, in turn, increases with decreasing distance, so it becomes stronger for the z component of the spins than for the x and y components. Thus the MnTe layers in our samples represent a 2D Heisenberg system with magnetic anisotropy which was demonstrated to show an Ising-like behavior, irrespective of how small the anisotropy is.²⁰ Furthermore, even without anisotropy 2D-Heisenberg systems change to 2D-Ising ones with increasing temperature.²¹

To discuss the consequences of the chosen approximations on the spin ordering it should be noted that without magnetic field and at $T = 0$ K, the ground state of bulk MnTe corresponds to an antiferromagnetic (AF)-III spin arrangement, which can be established only with finite values of the next-nearest-neighbor exchange interaction J_2 . Furthermore, at least 4 ML's MnTe have to be involved to end up with a complete AF-III spin arrangement, as shown in Fig. 1. By making the transition from the 3D to the 2D case there are two obvious possible spin configurations for a (100) oriented monolayer MnTe: (i) all spins are oriented in the plane of the magnetic layer, referred as the XY model, and (ii) all individual spins are pointing either upwards or downwards perpendicular to the magnetic layer, establishing a 2D AF-I ordering. In the first case each Mn ion is surrounded by four nearest neighbors (NN's), two with parallel and two with antiparallel spins, and four next-nearest neighbors (NNN's), again with two parallel and two antiparallel spins. For this case the phase-transition temperature, evaluated within the mean-field approximation by

$$kT_N = \frac{2}{3} S(S+1) [z_1 J_1 \cos \alpha + z_2 J_2 \cos \beta], \quad (2)$$

with z_1 , z_2 , the number of NN's and NNN's, J_1 (J_2), the exchange integrals for NN's (NNN's), and α (β) being the angle between the corresponding spin directions, vanishes. For the 2D AF-I ordering, in contrast, all four NN's are an-

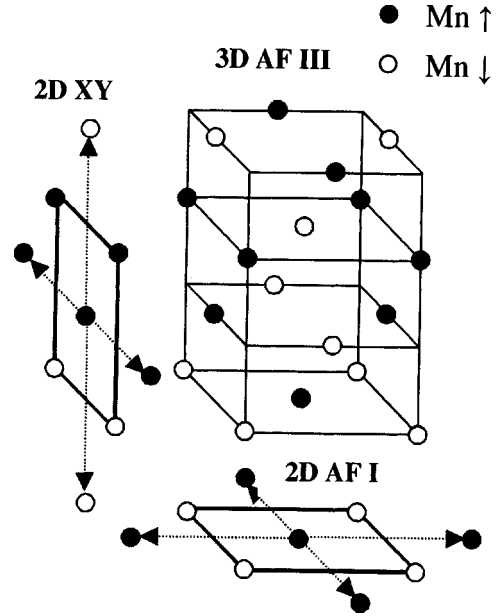


FIG. 1. Spin ordering of bulk MnTe (AF III) and 2D MnTe arrangements (2D AF-I and XY model). The dashed arrows indicate the next-nearest neighbors.

tiparallel oriented in respect to the central spin as well as to all four NNN's so that a finite Néel temperature of

$$T_N = \frac{8}{3k} S(S+1) [J_1 - J_2] \quad (3)$$

can be expected. Thus the 2D AF-I ordering, well approximated by the Ising model, is favorable in comparison to the XY ordering as long as J_2 is smaller than J_1 , implementing that in the 2D case neglecting J_2 does not affect the spin ordering as it would be the case in 3D.

To calculate the ground-state energy and magnetization, we perform a Monte Carlo simulation by using the Metropolis (heat bath) algorithm.²² The simulation is performed for a two-dimensional cubic lattice with a size up to 150×150 lattice sites and periodic boundary conditions. The magnetization is calculated after each Monte Carlo step by summing over all lattice spins whereas the energy is given by explicitly summing over all terms in Eq. (1). The energy and the magnetization given in the figures below result from averaging the results obtained from many Monte Carlo steps. The heat capacity c_H is calculated from the variance $(\Delta E)^2$ of the energy from one Monte Carlo micro state to the next, by using the fluctuation-dissipation theorem:

$$c_H = \frac{(\Delta E)^2}{k_B T^2}, \quad (4)$$

with the Boltzmann constant k_B and the temperature T . Furthermore, all results were checked to be independent from the chosen lattice size and the results for Mn concentrations in the two-dimensional lattice x_{Mn} smaller than 100% were averaged over 100 configurations with different randomly occupied lattice sites. All simulations were started with a perfect antiferromagnetic ordering of the magnetic ions,

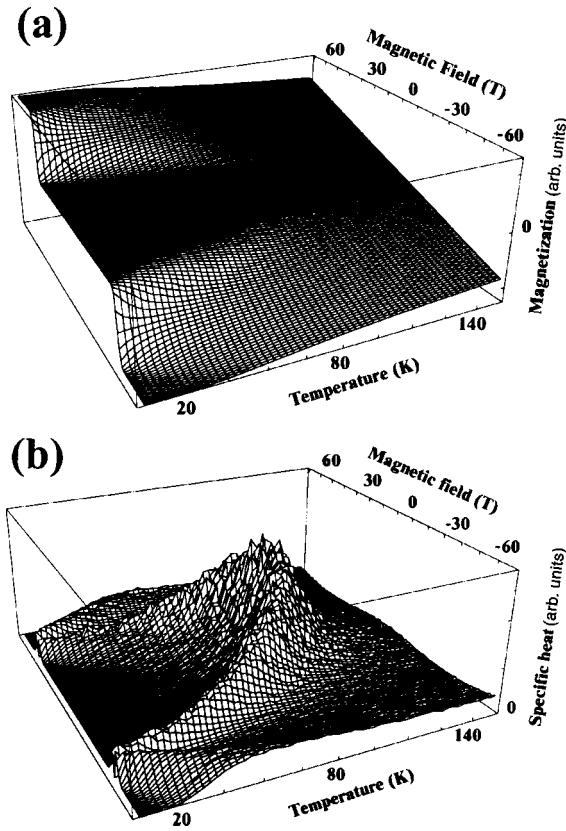


FIG. 2. Magnetization and specific heat for a purely two-dimensional MnTe layer as function of temperature and magnetic field. Here nearest-neighbor exchange interactions are taken into account.

whereas the final spin configuration is given after a sufficient number of Monte Carlo steps, when only small changes in energy are observed between subsequent steps.

Results of the Monte Carlo simulation performed for a 100% Mn occupation of the two-dimensional lattice and a value of the exchange integral of $J = -6.3k_B$ for MnTe (Ref. 23) are given in Fig. 2. As expected for an antiferromagnetic system, the magnetization is found to be zero at low temperatures and magnetic fields below a critical value of 45 T. In contrast, at a temperature of 150 K the magnetization shows a linear dependence on magnetic field, as expected for a paramagnetic system. The borderline between antiferromagnetic and paramagnetic regions in this magnetic-field-temperature map can be observed clearly by inspecting the specific heat in Fig. 2(b), which is expected to diverge at the antiferromagnetic-paramagnetic phase transition. In our simulation, the specific heat shows just a maximum at the phase transition instead of infinity, due to the finite size of the chosen two-dimensional lattice. Without magnetic field, this peak is observed around 90 K, a value which is substantially higher than the Néel temperature in bulk ZB MnTe. An increase of the phase-transition temperature in thin MnTe layers with respect to bulk was indeed observed by neutron-scattering experiments performed on superlattice samples,¹⁶ confirming our theoretical findings. The maximum in c_H as a function of B in Fig. 2(b) gives the complete phase diagram

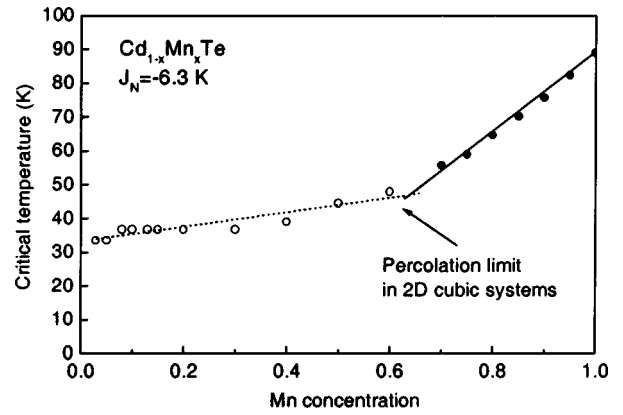


FIG. 3. Critical temperature as a function of the Mn concentration, obtained from the calculated maximum of the specific heat at zero field (filled dots correspond to a phase transition while the open circles indicate the breaking up of finite antiferromagnetically coupled clusters).

of the two-dimensional MnTe layer. It is worth noting that the phase diagram and thus the calculated Néel temperature depends not only on the choice of the exchange integral J , but is also influenced by exchange interactions with second and third nearest neighbors, neglected in the present simulation. The error by neglecting NNN interactions can directly be estimated by the use of Eq. (3) to be smaller than 10%, since J_1/J_2 is in the order of 10,²⁴ and because the contribution of NNN's causing a reduction of T_N is partially canceled by finite higher terms proportional to J_3 and J_4 .²⁵

As a next step, we repeated the simulation described above for Mn concentrations varying between 0 and 100%. In Fig. 3, the critical temperatures are given as obtained from the maximum in the specific heat at zero magnetic field. This maximum indicates the critical behavior of the magnetic system. By decreasing the Mn concentration, the critical temperature linearly decreases from 90 K at 100% occupation to 45 K at about 60%. Below this critical concentration again a linear decrease is observed, with a smaller slope, however. This critical concentration of 60%, where clearly a knee occurs in the concentration dependence of the critical temperature, is close to the theoretical percolation limit in a purely two-dimensional, cubic system.²⁶ So, above the critical concentration the peak in the heat capacity can be ascribed to an antiferromagnetic-paramagnetic phase transition, whereas below this critical value no long-range spin ordering is possible. There, the critical enhancement of the heat capacity is caused by the breaking up of finite, antiferromagnetically ordered clusters of magnetic ions causing deviations from a purely paramagnetic Curie-Weiss behavior. To show in Fig. 3 clearly that in the latter case no macroscopic phase transition occurs, the corresponding data points are plotted by open circles, in contrast to the phase-transition temperatures which are shown by filled dots.

III. ZEEMAN SPLITTING IN QUANTUM WELLS WITH INSERTED MnTe LAYERS

Due to the relatively small number of magnetic ions it is rather hard to directly probe the magnetization of a single

antiferromagnetic monolayer buried in a semiconductor heterostructure by conventional magnetometers. The Zeeman splitting induced by *sp-d* exchange interactions between the spins of free carriers and the localized magnetic ions, in contrast, can be clearly measured by magneto-optical spectroscopy, even for quantum well samples containing a fraction of a ML MnTe. The Zeeman splitting ΔE of electrons in semimagnetic samples can be written as²⁷

$$\Delta E = \sum_i \langle \Phi | S_i^z | \Phi \rangle A \Omega_0 |\psi_e(R_i)|^2, \quad (5)$$

where the electron wave function is separated into a purely spin-dependent part Φ and a spatially dependent part ψ . S_i^z is the component of the Mn spin operator in direction of the external magnetic field, A is the exchange constant, and Ω_0 the volume of the unit cell, and R_i represents the location of the magnetic ions. For quantum wells, the electron wave function can be separated into a lateral and a vertical part, $\psi_e(r=R_i) = \varphi_e(X_i, Y_i) \xi_e(Z_i)$. In our samples with single inserted Mn layers, Z_i has the same value for all Mn ions. Therefore the Zeeman splitting is directly proportional to the vertical part of the probability density at the location of the magnetic ions $|\xi_e(Z_i)|^2$. In an antiferromagnetic system the expectation value of the spin is strongly varying from lattice site to lattice site, whereas variations of the wave function of photoexcited electrons in lateral direction take place on much larger length scales, comparable to the exciton Bohr radius. Therefore Eq. (5) can be approximated by using an average value of the lateral dependence of the probability density in front of the summation. The Zeeman splitting becomes directly proportional to the magnetization of the layer M_l :

$$\begin{aligned} \Delta E &= A \Omega_0 |\xi_e(Z_{\text{Mn}})|^2 |\overline{\varphi_e(X_i, Y_i)}|^2 \sum_i \langle \Phi | S_i^z | \Phi \rangle \\ &= C |\xi_e(Z_{\text{Mn}})|^2 M_l. \end{aligned} \quad (6)$$

For the holes an analogous expression can be derived, however, with another proportionality factor C , to account for the larger value of the exchange integral. The exciton spin splitting probed in our experiments corresponds to the Zeeman splitting of the holes plus that of the electrons, so it is also directly proportional to M_l .

For a first check of our model, we compare the calculated values of the magnetization of a two-dimensional MnTe layer with the exciton Zeeman splitting in bulk $\text{Cd}_{1-x}\text{Mn}_x\text{Te}$ described in the literature.^{17,28,29} Both quantities are drawn as function of the Mn concentration. They exhibit a similar dependence up to a concentration of 73%, as shown in Fig. 4, even though the calculation is performed for a purely two-dimensional system and the experimental data are obtained by extrapolating the values for bulk material to a field of $B = 6$ T. The maximum of both values is observed at a Mn content around 20%. It should be noted that the theoretical values are normalized in order to fit the experimental data which are taken at a temperature far below the critical temperature for all Mn concentrations. There, the magnetization exhibits only a small dependence on the dimensionality of

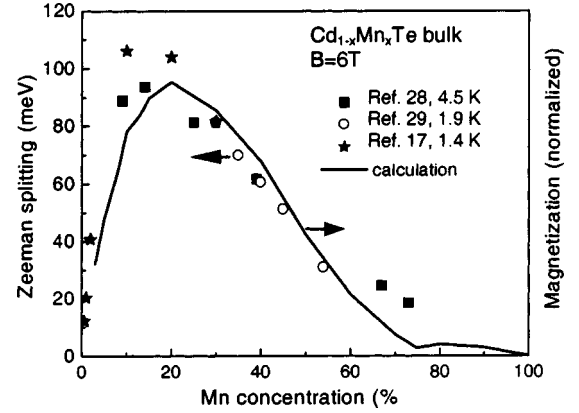


FIG. 4. Comparison between the Zeeman splitting obtained from experiments on bulk $\text{Cd}_{1-x}\text{Mn}_x\text{Te}$ (dots) and from the magnetization calculated for a purely two-dimensional system (line).

the magnetic system.³⁰ The reason for the scattering of the experimental data in Fig. 4, taken from different references, is caused by the slightly different sample temperatures ranging between 1.4 and 4.5 K.

Up to now, the concentration dependence of the magnetization and thus of the exciton Zeeman splitting was described by the use of a modified Brillouin function $B_{5/2}$,

$$\Delta E = (\beta - \alpha) N_0 x S_0 B_{5/2} \left(\frac{5/2 g \mu_B}{k T_{\text{eff}}} \right), \quad (7)$$

introduced by Gaj *et al.*¹⁷ with two phenomenological parameters, the saturation spin S_0 and an effective temperature T_{eff} . Here α and β are the exchange integrals for the conduction and the valence band, N_0 is the number of unit cells per unit volume, and x is the Mn concentration. Instead of the saturation spin often rather an effective concentration $\bar{x} = x S_0 / S$ is used as empirical parameter for fitting the magnetic-field dependence of the exciton Zeeman splitting. Here we want to stress that (i) both effective quantities, T_{eff} and \bar{x} , depend strongly on the actual Mn concentration, and (ii) we do not use these quantities in our model. Even when the concentration dependence of the exciton Zeeman splitting is used to determine the dependence of \bar{x} on the actual concentration x (e.g., by assuming a constant value of T_{eff}), Eq. (7) is still not adequate to fit our experimental results, because it does not allow us to describe any magnetic phase transition.

IV. SAMPLES AND EXPERIMENTAL DETAILS

We have determined the magnetization of quasi-two-dimensional MnTe layers in two different samples. Both samples are 48-Å wide CdTe quantum wells with $\text{Cd}_{0.85}\text{Mg}_{0.15}\text{Te}$ barriers, grown by molecular-beam epitaxy on (001) oriented $\text{Cd}_{0.96}\text{Zn}_{0.04}\text{Te}$ substrates. Sample 1 (S1) contains a single ML MnTe in the center of the well, while two MnTe barriers with a half ML coverage and an equidistant spacing within the well are embedded in sample 2 (S2). The growth of the quantum wells was performed with a very slow rate of 8 s/ML in order to control the Mn incorporation

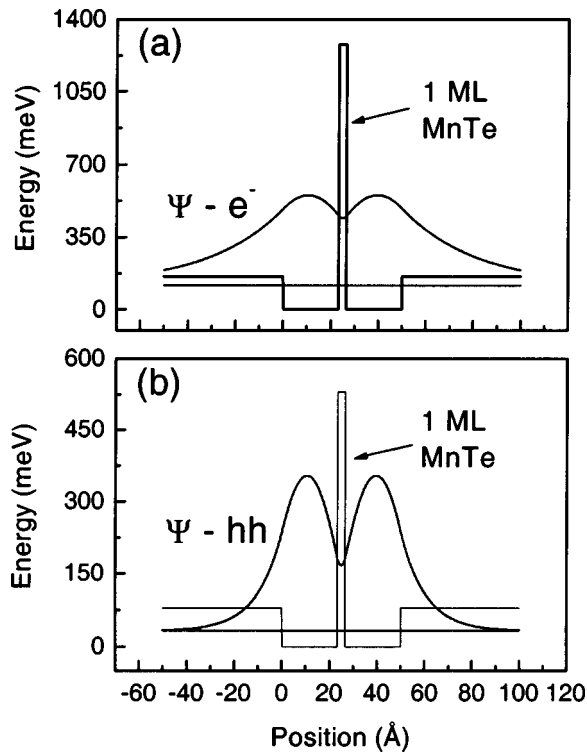


FIG. 5. Conduction band and valence band of sample S1, that has a 48-Å-wide CdMgTe/CdTe quantum well with nominally 1 ML MnTe in its center. The electron and heavy hole wave function are shown together with the corresponding ground-state energy levels.

precisely. Each interface was smoothed by performing growth interruptions under Te excess and the layer by layer growth was monitored by reflection high-energy electron diffraction (RHEED) oscillations.

For clarity, the conduction and valence band edges of S1 are indicated in Fig. 5, together with the electron and heavy-hole ground-state energies and the corresponding wave functions. The calculation is performed using a valence-band offset of 0.33, with the effective masses for the electrons of $m_e^* = 0.096 m_0$ and the heavy holes $m_{hh} = 0.63 m_0$,^{31,32} and a band gap for Cd_{1-x}Mg_xTe of $E_G = (1.606 + 1.654x)$ eV,³³ and for Cd_{1-x}Mn_xTe of $E_{G'} = (1.606 + 1.592x)$ eV (Ref. 34) (m_0 is the free-electron mass). Figure 5 clearly shows that the wave function of the electrons as well as that of the holes penetrates to some extent into the magnetic MnTe layer. Due to this penetration, optically generated excitons in the quantum well are able to interact with the localized magnetic ions in the MnTe barriers, leading to a drastic increase of the exciton spin (Zeeman) splitting in external magnetic fields. As shown above, the spin splitting is directly proportional to the magnetization of the sample. Thus the magnetization of single magnetic monolayers can be probed by magneto-optical spectroscopy detecting the exciton spin splitting.

The magneto-optical experiments were performed in Faraday configuration where optical transitions are allowed only for circular polarized light with positive or negative helicity.¹⁸ As light source for the photoluminescence (PL), and PL excitation (PLE) experiments, a tunable dye laser

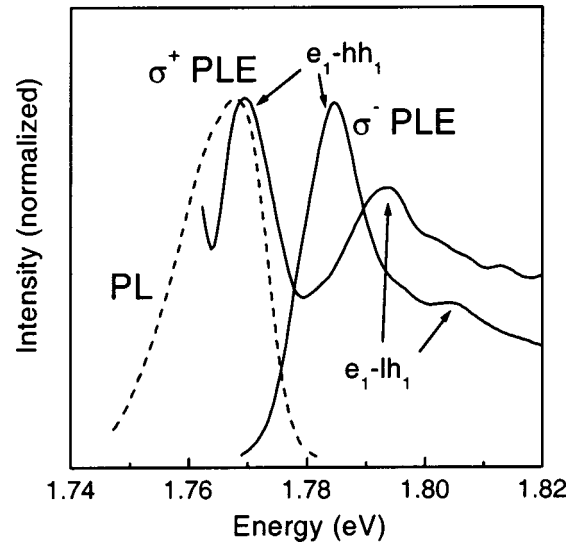


FIG. 6. Photoluminescence (PL) spectrum and PL excitation (PLE) spectra of sample S1 obtained at $T = 1.7$ K and $B = 3$ T with circularly polarized light. The PLE spectra allow us to determine the transition energy between the electron ground state e_1 and the ground states of the heavy holes hh_1 and light holes lh_1 .

operating in the wavelength range between 620 and 800 nm was used in combination with a Fresnel rhombus as achromatic polarizer. The samples were mounted in the center of a split-coil magnet cryostat with a variable temperature inset allowing us to control the temperature at the position of the sample with an accuracy better than 0.5 K. For PL and PLE measurements the excitation power was kept below 1 mW to avoid additional sample heating at the laser spot.

V. EXPERIMENTAL RESULTS AND DISCUSSION

In the following we present the results of the magneto-optical experiments for samples S1 and S2. At a temperature of 1.7 K both samples exhibit Gaussian-shaped PL lines with a full width at half maximum of about 12 meV. For a magnetic field of 3 T the PL spectrum of S1 is shown in Fig. 6 together with the PLE spectra obtained for excitation with circularly polarized light with positive (σ^+) and negative (σ^-) helicity, detected at the wavelength corresponding to the maximum of the PL spectrum. For both orientations of the polarization the excitonic transition between the ground states of the electrons (e_1) and the heavy holes (hh_1) can be clearly identified. At a field of 3 T this transition exhibits a Zeeman splitting of 16 meV. At higher energies additional peaks are detectable in Fig. 6, caused either by an excitonic transition involving the ground state of the light holes (e_1 - lh_1) or due to excitons corresponding to higher heavy holes states.

The energies of the e_1 - hh_1 exciton transitions of samples S1 and S2 as a function of magnetic field are given in Fig. 7 for a temperature of 1.7 K. Although both quantum well samples have the same well width and composition of the barriers and contain the same amount of Mn ions, the PLE transition energies are found to be substantially different in two respects: (i) At zero magnetic field, the e_1 - hh_1 transition

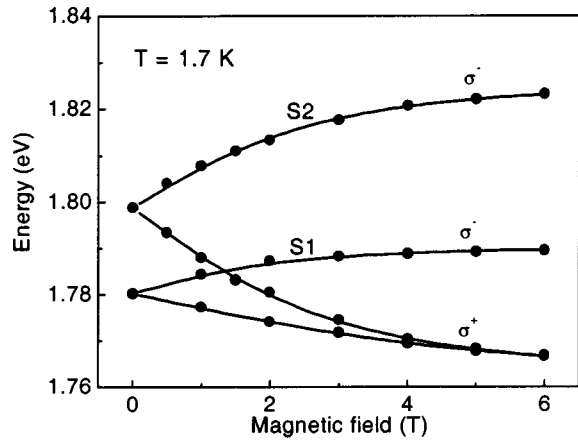


FIG. 7. Zeeman splitting of the e_1 - hh_1 exciton transition of sample S1 and S2 deduced from PLE spectra.

energy of sample S1 is about 2 meV smaller than that of S2; (ii) in magnetic fields, the Zeeman splitting of sample S2 is more than twice as large as for S1, indicating a much higher content of paramagnetic Mn ions of 2.4% in S2 as compared to 0.9% in S1.³⁵ So in both samples the fraction of paramagnetic ions averaged over the quantum well region is clearly smaller than the total Mn content of 6%. Thus the reason for the different spin splitting is the antiferromagnetic coupling between the magnetic ions, which is reduced in S2 where the Mn ions are distributed in two separate layers, in comparison to S1 that contains only one layer with the same amount of magnetic ions. The different transition energies at zero field, in turn, can be explained by the different barrier profiles in sample S2 and S1. The observed transition energies are consistent with calculations where the barrier profiles are approximated by a Gaussian function, taking into account the Mn distribution in growth direction by choosing a barrier width of 1.25 ML's for S1.³⁵

Basically, antiferromagnetically coupled Mn ions exhibit a completely different temperature dependence of their magnetization than paramagnetic ions. Therefore we study the temperature dependence of the exciton Zeeman splitting, probing the magnetization induced by the MnTe insertions. Obviously, the Zeeman splitting decreases with increasing temperature as it is directly seen from the PLE spectra in Fig. 8. There, the σ^- polarized PLE spectra of sample S1 at 6 T and 1.7 K are shown for three different temperatures. As a main feature the high-energy branch of the e_1 - hh_1 transition shows a 6-meV redshift when the temperature increases from 15 to 35 K, being a direct consequence of the decreasing exciton Zeeman splitting, taking into consideration that the band gap of CdTe shrinks only 2 meV within this temperature range.³⁶

The temperature dependence of the inverse Zeeman splitting ($1/\Delta E$) of the e_1 - hh_1 exciton transition is shown in detail in Fig. 9. For sample S1, $1/\Delta E$ increases linearly when the temperature increases up to 50 K. At about 50 K, $1/\Delta E$ versus T levels off, up to a temperature of 100 K. Above this temperature, the slope increases and again an almost linear dependence is observed (see Fig. 9). In sample S1, the spin splitting unambiguously could be observed by the PLE ex-

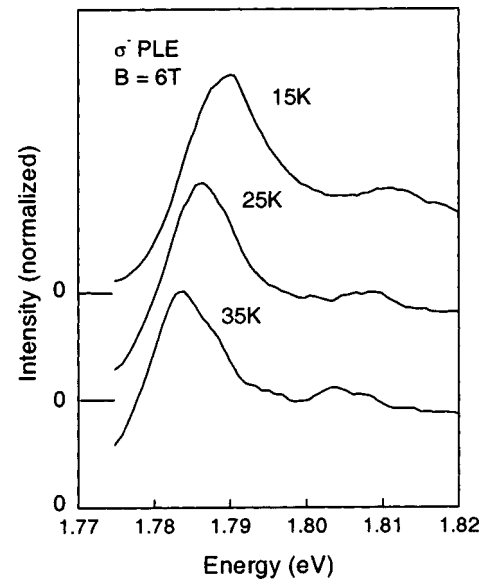


FIG. 8. σ^- polarized photoluminescence excitation spectra of sample S2 at three different temperatures.

periments up to a temperature of 140 K. For sample S2 in comparison, only one kink is detected at about 40 K in the otherwise linear temperature dependence of $1/\Delta E$ (see Fig. 10). For both samples the temperature dependence of the inverse Zeeman splitting clearly deviates from a paramagnetic Curie-Weiss behavior predicting a linear increase of $1/\Delta E$ with increasing temperature. This deviation on one hand confirms the presence of antiferromagnetically coupled Mn ions in both samples and on the other hand allows to determine quantitatively the Mn distribution profile in growth direction for both samples.

In order to simulate the observed temperature dependencies of the inverse Zeeman splitting two effects have to be taken into account: (i) the actual Mn distribution resulting from the insertion of a single or $\frac{1}{2}$ ML MnTe due to diffusion in growth direction, and (ii), the increase of the exciton Zeeman splitting due to sp - d exchange interactions. To take into account both effects, we approximate the Mn distribution

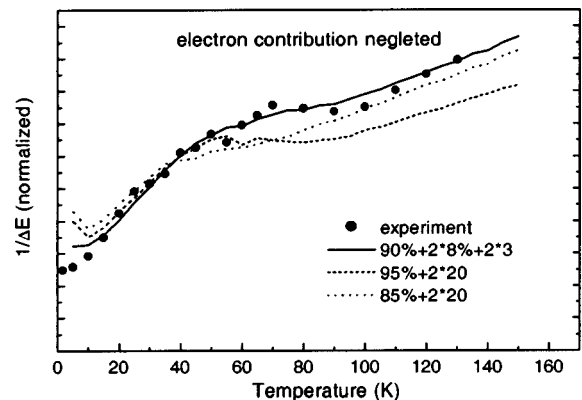


FIG. 9. Temperature dependence of the inverse Zeeman splitting of sample 1 at 1.7 K and 6 T obtained from the photoluminescence excitation spectra (dots). The lines are results of simulations performed for different steplike MnTe distribution profiles.

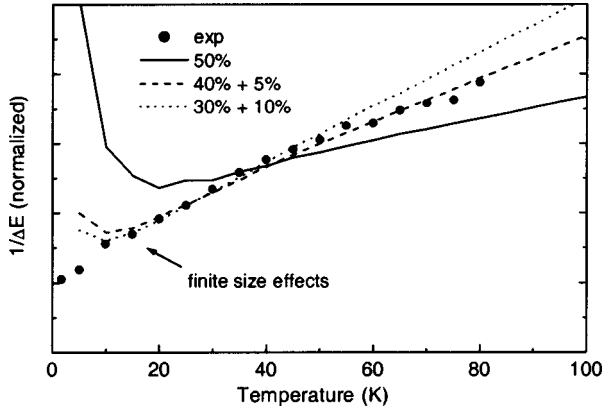


FIG. 10. Inverse Zeeman splitting measured and simulated for sample S2. The simulation deviates at low temperatures from the data points due to finite-size effects.

profile of the inserted layer by a steplike function consisting of 1 ML with high Mn concentration accompanied by 2 ML's with by far smaller Mn concentrations on each side. Such an arrangement allows us, e.g., to approximate an Gaussian distribution, as indicated in Fig. 11. The inverse Zeeman splitting is then calculated by summing over the contributions of each individual layer, by

$$\frac{1}{\Delta E} = \frac{\text{const}}{\sum_j M_{I_j} |\xi(Z_{\text{Mn}}^j)|^2}. \quad (8)$$

The inverse Zeeman splitting, calculated as function of temperature, sensitively depends on the chosen Mn distribution profile (see curves in Fig. 9). Best agreement with the experimental data is obtained for a Mn distribution approximated by 1 ML with 90% Mn concentration with two neighboring ML's with 8% Mn embedded inbetween two additional ML's with 3% Mn. As can be seen, the simulations performed with other combinations of magnetic layers yield qualitatively similar dependencies, but normalizing the results does not allow us to approximate the different slopes of

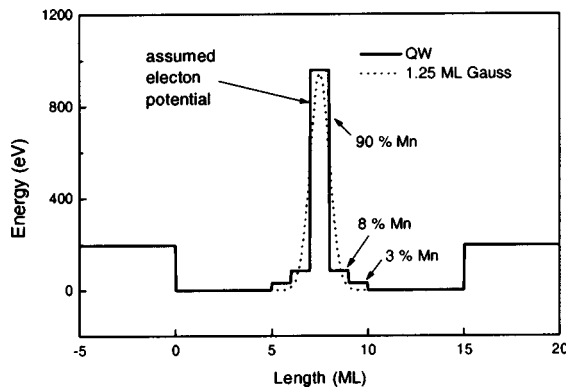


FIG. 11. Conduction-band edge of sample S1: The shown step-like Mn distribution profile gives the best agreement between the simulated temperature dependence of the inverse Zeeman splitting and the experimental ones. It can be well approximated by a Gaussian profile (dotted line) with the same amount of Mn and a width of 1.25 ML's.

$1/\Delta E$ as function of T over the whole temperature range. Similar to this, for the sample containing $\frac{1}{2}$ ML MnTe the experimental data can be approximated well by using 1 ML with 40% Mn accompanied by two layers with 5%, but not with other Mn distributions. Therefore fitting the temperature dependence of the inverse Zeeman splitting allow us to determine the approximate Mn diffusion profile of the inserted magnetic layers. Indeed the combination of $\text{Cd}_{1-x}\text{Mn}_x\text{Te}$ ML's determined for S1 is a good approximation for a Gaussian spin distribution with a width of 1.25 ML's, as determined in our previous work for the same sample³⁵ by a different method, again confirming the presence of ultrathin antiferromagnetic layers in our quantum well samples. This spin distribution is rather narrow, considering the interface roughness parameter of about 7 Å as determined from x-ray scattering experiments performed on CdTe/MnTe superlattices³⁷ or by assuming a strictly exponential segregation of the Mn ions during growth.^{38,39} For quasi-two-dimensional $\text{Zn}_{1-x}\text{Mn}_x\text{Se}$ layers digitally inserted in single $\text{ZnSe}/\text{Zn}_{0.8}\text{Cd}_{0.2}\text{Se}$ quantum wells, however, already similar narrow Mn distributions have been demonstrated⁸ and also other numerical methods⁴⁰ allowed us to simulate the interface between a diluted magnetic semiconductor and a non-magnetic quantum well by considering only contributions from two magnetic monolayers.^{41,42} In addition to the Mn distribution profile, from our simulated results the critical temperature can be determined. For sample S1, it is found to be around 70 K, in between the two kinks in the temperature dependence of the inverse Zeeman splitting shown in Fig. 8, whereas in S2 no phase transition occurs.

Finally we want to address the error of our method by neglecting the antiferromagnetic coupling to adjacent magnetic layers. An upper limit for this error is given just by the number of neighbors in the adjacent layer, which accounts for about 15% of the determined Mn distribution profile. Certainly the error represents an upper limit, because the Mn-Mn interaction corresponding to a temperature of 6.3 K is small compared to the temperature range which was used for fitting the experimental data. Therefore it is roughly as large as the error obtained by neglecting in-plane interactions involving second and third nearest neighbors, as it is discussed above.

VI. SUMMARY

The temperature-dependent magnetization of quantum well samples containing ultrathin layers of MnTe is studied by polarization-dependent photoluminescence excitation experiments. For these samples, the inverse Zeeman splitting, which is proportional to the inverse magnetization, clearly shows a non-Curie-Weiss temperature dependence due to antiferromagnetic coupling between the magnetic Mn ions. In particular, up to two kinks are observed in the otherwise linear temperature dependencies, which allows us to determine the critical temperature where the paramagnetic-antiferromagnetic phase transition takes place. Fitting the experimental temperature dependencies enables us to determine an approximate Mn distribution profile, resulting from the inserted MnTe sub-monolayers. For this purpose,

the temperature- and magnetic-field-dependent magnetization of a purely two-dimensional arrangement of Mn ions was calculated by a Monte Carlo simulation. The increase of the exciton Zeeman splitting due to *sp-d* exchange interactions between localized magnetic moments and that of the free electrons is fully taken into account. The approximate Mn diffusion profile, consisting of one two-dimensional layer with a Mn content of 90% and two neighboring layers with 8%, and two further layers with 3% obtained for a sample nominally containing one single monolayer MnTe, is

in good agreement with previous diffusion profiles, deduced from alternative experimental techniques.³⁵

ACKNOWLEDGMENTS

We want to thank J. Jägermüller, W. Krepper, and O. Fuchs for technical assistance. This work was supported by the “Fonds zur Förderung wissenschaftlicher Forschung, FWF” and by the ÖAD in Austria.

- ¹K. G. Wilson, *Sci. Am.* **241** (2), 140 (1979).
- ²For an overview see, for example, J. K. Furdyna and J. Kossut, *Diluted Magnetic Semiconductors, Semiconductor and Semimentals*, edited by R. K. Willardson and A. C. Beer (Academic, New York, 1988), Vol. 25.
- ³Z. Q. Qiu, J. Pearson, and S. D. Bader, *Phys. Rev. Lett.* **12**, 1646 (1991).
- ⁴C. H. Back, Ch. Wursch, A. Vaterlaus, U. Rampsen, U. Maier, and D. Pescia, *Nature (London)* **378**, 597 (1995).
- ⁵J. C. Campuzano, M. S. Foster, G. Jennings, R. F. Willis, and W. Unertl, *Phys. Rev. Lett.* **54**, 2684 (1985).
- ⁶W. Duerr, M. Tadorelli, O. Paul, R. German, W. Gudat, D. Pescia, and M. Landolt, *Phys. Rev. Lett.* **62**, 206 (1989).
- ⁷J. Eymery, J. M. Hartman, and G. T. Baumbach, *J. Appl. Phys.* **87**, 7266 (2000).
- ⁸S. A. Crooker, N. Samarth, and D. D. Awschalom, *Phys. Rev. B* **61**, 1736 (2000).
- ⁹S. A. Crooker, D. A. Tulchinsky, J. Levy, D. D. Awschalom, R. Garcia, and N. Samarth, *Phys. Rev. Lett.* **75**, 505 (1995).
- ¹⁰R. K. Kawakami, E. Johnson-Halperin, L. F. Chen, M. Hanson, N. Guébels, J. S. Speck, A. C. Gossard, and D. D. Awschalom, *Appl. Phys. Lett.* **77**, 2379 (2000).
- ¹¹Ch. V. Mohan, H. Kronmüller, and M. Kelsch, *Phys. Rev. B* **57**, 2701 (1998).
- ¹²R. P. Michel, A. Chaiken, M. A. Wall, J. W. Dykes, J. F. Ankner, and H. Kaiser, *J. Appl. Phys.* **79**, 4775 (1996).
- ¹³H. Yamazaki, *Phys. Status Solidi B* **197**, 195 (1996).
- ¹⁴H. Kepa, K. I. Goldman, T. M. Giebultowicz, C. F. Majkrzak, G. Springholz, H. Krenn, S. Holl, F. Schinagl, and G. Bauer, *Photonics Spectra* **2**, 399 (1998).
- ¹⁵P. Anderson, *Phys. Rev.* **79**, 705 (1950).
- ¹⁶T. M. Giebultowicz, P. Klosowski, N. Samarth, H. Luo, J. K. Furdyna, and J. J. Rhyne, *Phys. Rev. B* **48**, 12817 (1993).
- ¹⁷J. A. Gaj, R. Planel, and G. Fishman, *Solid State Commun.* **29**, 435 (1979).
- ¹⁸D. U. Bartholomew, J. K. Furdyna, and A. K. Ramdas, *Phys. Rev. B* **34**, 6943 (1986).
- ¹⁹J. Esser, U. Nowak, and K. D. Usadel, *Phys. Rev. B* **55**, 5866 (1997).
- ²⁰M. Bander and D. L. Mills, *Phys. Rev. B* **38**, 12015 (1988).
- ²¹V. Yu. Irkhin and A. A. Katanin, *Phys. Rev. B* **57**, 379 (1998).
- ²²N. Metropolis, A. W. Rosenbluth, M. N. Rosenbluth, A. H. Teller, A. H. Teller, and E. Teller, *J. Chem. Phys.* **21**, 1087 (1953).
- ²³J. Spalek, A. Lewicki, Z. Tarnawski, J. K. Furdyna, R. R. Galazka, and Z. Obuszko, *Phys. Rev. B* **33**, 3407 (1986).
- ²⁴T. M. Giebultowicz, J. J. Rhyne, W. Y. Ching, D. L. Huber, J. K. Furdyna, B. Lebeck, and R. R. Galazka, *Phys. Rev. B* **39**, 6857 (1989).
- ²⁵A. Bruno and J. P. Lascaray, *J. Cryst. Growth* **101**, 936 (1990).
- ²⁶K. Takeda, Y. Okuda, I. Yamada, and T. Haseda, *J. Phys. Soc. Jpn.* **50**, 1917 (1981).
- ²⁷G. Precht, W. Heiss, A. Bonanni, W. Jantsch, E. Janik, and G. Karczewski, *Phys. Rev. B* **61**, 15617 (2000).
- ²⁸J. P. Lascaray, D. Coquillat, J. Deportes, and A. K. Battacharjee, *Phys. Rev. B* **38**, 7602 (1988).
- ²⁹G. Rebmann, C. Rigaux, G. Bastard, M. Menant, R. Tribulet, and W. Giriat, *Physica B & C* **117B&118B**, 452 (1983).
- ³⁰This can be directly seen from magnetization experiments done on ferromagnetic multilayers, shown, e.g., in A. Stachow-Wójcik, T. Story, W. Dobrowolski, M. Arciszewska, R. R. Galazka, M. W. Kreijveld, C. H. W. Swüste, H. J. M. Swagten, W. J. M. de Jonge, A. Twardowski, and A. Yu. Sipatov, *Phys. Rev. B* **60**, 15220 (1999).
- ³¹K. K. Kanazawa and F. C. Brown, *Phys. Rev.* **135 A**, 1757 (1964).
- ³²R. Wojtal, A. Golnik, and J. A. Gaj, *Phys. Status Solidi B* **96**, 241 (1979).
- ³³D. Tönnies, G. Bacher, A. Forchel, A. Waag, and G. Landwehr, *Appl. Phys. Lett.* **64**, 766 (1994).
- ³⁴J. K. Furdyna, *J. Appl. Phys.* **64**, R29 (1988).
- ³⁵G. Precht, W. Heiss, S. Mackowski, A. Bonanni, G. Karczewski, H. Sitter, and W. Jantsch, *Semicond. Sci. Technol.* **15**, 506 (2000).
- ³⁶J. Camassel, D. Auvergne, H. Mathieu, R. Triboulet, and M. Vargaftik, *Solid State Commun.* **13**, 63 (1973).
- ³⁷J. Eymery, J. M. Hartmann, and G. T. Baumbach, *J. Appl. Phys.* **87**, 7266 (2000).
- ³⁸W. Grieshaber, A. Haury, J. Cibert, Y. Merle d'Aubigné, A. Wasiela, and J. A. Gaj, *Phys. Rev. B* **53**, 4891 (1996).
- ³⁹J. A. Gaj, W. Grieshaber, C. Bodin-Deshayes, J. Cibert, G. Feuillet, Y. Merle d'Aubigné, and A. Wasiela, *Phys. Rev. B* **50**, 5512 (1994).
- ⁴⁰T. Stimer, J. M. Fatah, R. G. Roberts, T. Piorek, W. E. Hagston, and P. Harrison, *Superlattices Microstruct.* **16**, 11 (1994).
- ⁴¹P. J. Klar, D. Wolverson, J. J. Davies, W. Heimbrodt, and M. Happ, *Phys. Rev. B* **57**, 7103 (1998).
- ⁴²J. M. Fatah, T. Piorek, P. Harrison, T. Stimer, and W. E. Hagston, *Phys. Rev. B* **49**, 10341 (1994).